Early Visual Cortex Supports One-Shot Episodic Memory via Spatially Tuned Reactivation

Robert Woodry[1], Jonathan Winawer[1,2], Serra E. Favila[3]

1 Department of Psychology, New York University, New York City, NY 10003

2 Center for Neural Science, New York University, New York City, NY 10003

3 Department of Cognitive and Psychological Sciences, Brown University, Providence, RI 02912

Acknowledgements: We thank New York University's Center for Brain Imaging for technical support. This research was supported by the National Institutes of Health (F99 NS105223 to S. Favila; R01 EY027401 to J. Winawer; P30 EY013079 Core grant for vision; R01 MH111417 to J. Winawer; T90 DA059110 computational neuroscience training grant supporting R. Woodry) and pilot grants from the NYU Center for Brain Imaging. This work was supported in part through the NYU IT High Performance Computing resources, services, and staff expertise.

Abstract

Episodic memory retrieval is thought to rely on the reactivation of prior perceptual representations in sensory cortex, a phenomenon known as cortical reinstatement. Support for this idea in early sensory areas comes from studies involving repeated exposure and explicit recall instructions. In everyday life, however, people often remember details from single events without repeated practice or instruction. We used fMRI to test whether memory responses emerge in early visual cortex after a single encoding event. Twenty adults viewed objects presented once in one of four parafoveal locations, then later completed recognition (old/new) and location recall tasks in which objects were shown foveally. We observed low amplitude responses in V1 to V3 during both memory tasks. These responses were tuned to the encoded parafoveal location, even though the recognition task did not ask the participant to remember the encoded location. These responses were more robust and precise for successfully remembered items, linking neural tuning in early visual cortex to one-shot memory performance. Our findings demonstrate that early visual cortex supports the defining property of episodic memory, the ability to retrieve sensory details from a single event.

Introduction

The ability to retrieve sensory details from a single experience is the defining property of episodic memory. This process is thought to rely on both the hippocampus and cerebral cortex – the hippocampus because of its capacity for rapid plasticity and cortex because its circuits can specify detailed sensory information. Models of episodic memory propose that, at least for new experiences, memories are stored in hippocampal circuits, and that during retrieval hippocampal activity leads to the reactivation of cortical populations that encoded the initial experience (Damasio, 1989; McClelland et al., 1995; Schacter et al., 1998). Reinstating cortical activity during retrieval is presumed to be useful for guiding behavioral responses.

Human neuroimaging studies leave little doubt that there is cortical reinstatement of sensory representations during retrieval (Kosslyn et al., 2001; Wheeler et al., 2000), and that this cortical activity carries stimulus-specific information, such as object category (Kuhl et al., 2011; Kuhl & Chun, 2014; Polyn et al., 2005) or stimulus location (Favila et al., 2022; Vo et al., 2022; Woodry et al., 2025). There is, however, equally little doubt that memory of sensory experience is imperfect and incomplete. People do not typically confuse memory and perception (Johns et al., 2004), and memories, particularly for single events, contain omissions and distortions (Schacter, 1999). Hence, it is perhaps surprising that many studies have reported robust and specific memory activity in the earliest stages of cortical processing, including primary visual cortex, or "V1" (Bone & Buchsbaum, 2021; Bosch et al., 2014; Breedlove et al., 2020; Favila et al., 2022; Favila & Aly, 2023; Naselaris et al., 2015; Vo et al., 2022; Woodry et al., 2025). However, these studies share two features which limit their generalizability to episodic memory of single events. First, prior to retrieval, participants were trained repeatedly on associations between a retrieval cue and the stimulus to be later retrieved. Second, during retrieval, participants were instructed to explicitly recall the images. Experiments with highly-trained associations and explicit retrieval instruction offer many advantages, such as high task performance and high signal-to-noise ratios in the neural measurements. However, they do not test the episodic memory system's foundational property: the ability to store and retrieve a unique, once-experienced event. Therefore, it is not known whether and how stimulus-specific memory reactivation in early visual cortex generalizes to memory for a single event.

Memory for a single event differs in many ways from memory for highly learned associations. For example, both study repetition (Young & Bellezza, 1982) and retrieval practice (Roediger & Butler, 2011) improve recall performance. Moreover, repetition can affect where and how memories are stored. With repetition, memory representations can shift from hippocampus to cortex (Frankland & Bontempi, 2005). These cortical representations are thought to be more gist-like, as they are built up by averaging over many related experiences (McClelland et al., 1995). Therefore, one cannot assume that features of retrieval, such as

cortical reinstatement, will generalize from highly practiced associations to one-shot experimental procedures. The question of generalization is especially pertinent for early sensory areas (such as V1), where involvement in higher level cognition remains controversial (Linton et al., 2024), and neuroimaging evidence for sensory reactivation has been less consistent than in higher level cortical areas (for a review, see (Kosslyn & Thompson, 2003).

Here, we used population receptive field (pRF) encoding models (Dumoulin & Wandell, 2008) to quantify cortical reinstatement in early visual cortex for once-experienced events. We scanned 20 subjects while testing their memory of parafoveal objects viewed once at one of four polar angles. We asked whether retrieval caused reactivation at the retinotopic location of the stimulus at encoding, and whether such reactivation was linked to memory behavior.

Results

We scanned 20 subjects while testing their memory for objects seen once parafoveally. Subjects encountered object images across three interleaved tasks (Figure 1). In the first task, *encoding*, they were shown trial-unique objects at one of four polar angles, two degrees away from fixation. In the second task, *recognition*, they viewed objects foveally and made old vs. new judgments. In the third task, *recall*, they viewed old objects foveally and reported the location at encoding. We used pRF models to measure spatial tuning in early visual cortex during perception and memory.

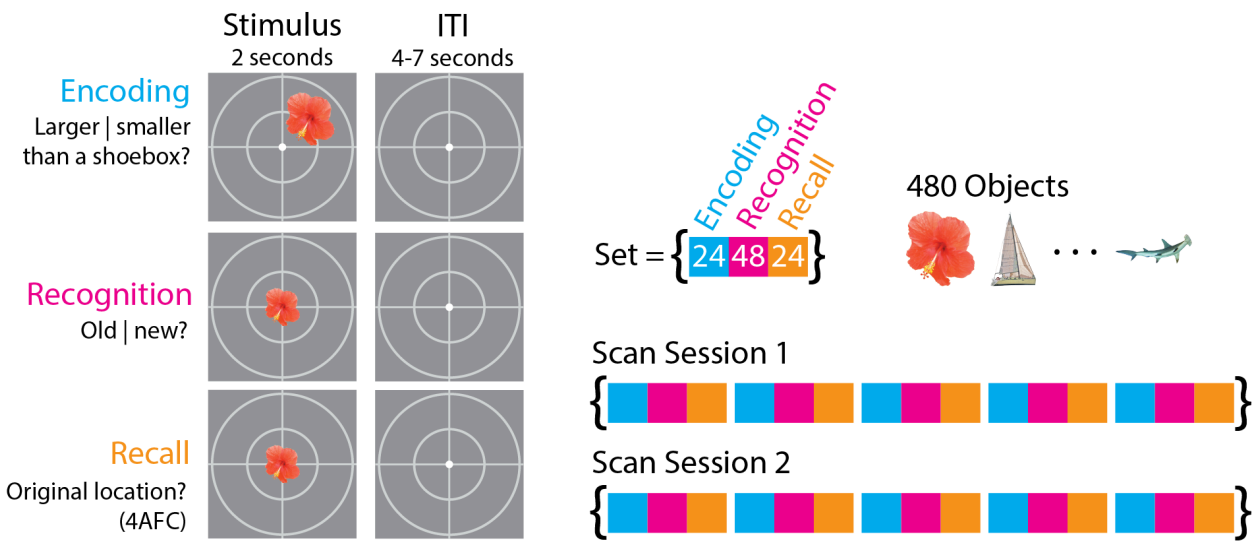

Figure 1. Experimental design

Subjects participated in two fMRI sessions with 15 scans each: encoding, recognition, and recall, repeated five times. The encoding and recall scans included 24 trials each, corresponding to 24 distinct objects, in random order. Recognition scans contained the same 24 objects, with an additional 24 new objects (lures), each shown at fixation in random order. In encoding trials, subjects were briefly shown an object in one of four locations at 2° eccentricity (45°, 135°, 225°, or 315° polar angle) and asked to indicate whether they were larger or smaller than a shoebox in real life. In recognition trials, subjects were shown an object at fixation and were asked to indicate whether it was old or new. In recall trials, subjects were shown an old object at fixation, and were asked to indicate its original location.

Memory performance for object recognition and spatial location recall

We first quantified performance on both the object recognition and the spatial location recall task. A goal in designing the experiment was that participants would be able to do the task (i.e., performance well above chance), but that performance on the location task would be far from perfect so that we could assess trial to trial variability in behavior and brain responses.

In the object recognition task, we computed the hit rate (percentage of old objects identified as 'old') and the false alarm rate (percentage of new objects misidentified as 'old') for each subject. An equal number of old and new objects presented during the object recognition task meant chance performance was at 50%. Subjects achieved an average hit rate of 90% [95 CI 87%, 92%], and an average false alarm rate of 7% [5%, 9%], indicating good but not perfect performance (Figure 2A). Hit and false alarm rates remained stable across scans (Figure 2C).

In the spatial location recall task, we computed the average accuracy for each subject. Because the task had four options — corresponding to the four potential locations objects could be presented at during the encoding task — chance performance was 25%. The average accuracy was 69% [95 CI 63%, 74%] (Figure 2B). Performance improved slightly from the first to the second block, and then remained stable (Figure 2D).

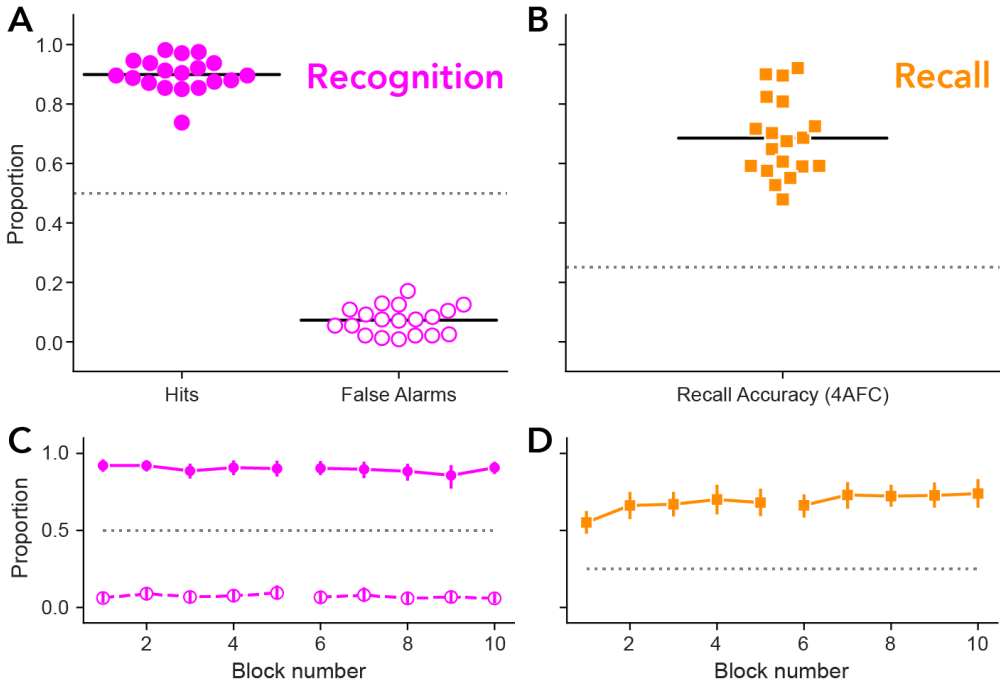

Figure 2. Behavioral performance on object recognition and spatial location recall tasks.
A) Subject-level performance on the object recognition task. Across all subjects (individual points), hit rate (solid pink) and false alarm rate (hollow pink) were well beyond chance (dotted gray line). Black horizontal bars indicate mean hit rate (left) and false alarm rate (right). B) Subject-level performance on the spatial recall task. Across all subjects (individual orange squares), mean performance was well above chance (dotted gray). Black horizontal bar indicates subject group mean. C) Group-level average performance on the object recognition task across blocks. Hit rate (solid pink) and false alarm rate (dashed pink) were stable and well beyond chance (dotted gray) across all blocks and the two sessions. Error bars indicate 95% CI obtained from 1000 bootstraps across subjects. D) Group-level average performance on the spatial recall task across blocks. Mean performance was stable and well beyond chance (dotted gray) across all blocks and the two sessions. Error bars indicate 95% CI obtained from 1000 bootstraps across subjects. The code and data to generate this and all subsequent figures can be found at https://osf.io/a9hkg/.

A single viewing is sufficient for spatially tuned memory responses in early visual cortex

Confident that our subjects could recognize the objects and retrieve their original locations after a single viewing, we next asked whether retrieving these object memories caused activity in visual cortex spatially tuned to the object's source location. We tested this hypothesis by using pRF models to project measures of brain activity from the surface of early visual cortex (V1-V3) to visual space (Figure 3A). From these we computed polar angle activation profiles for

each visual map and task, and quantified each profile's spatial tuning by computing its peak location, amplitude, tuning width, and fidelity.

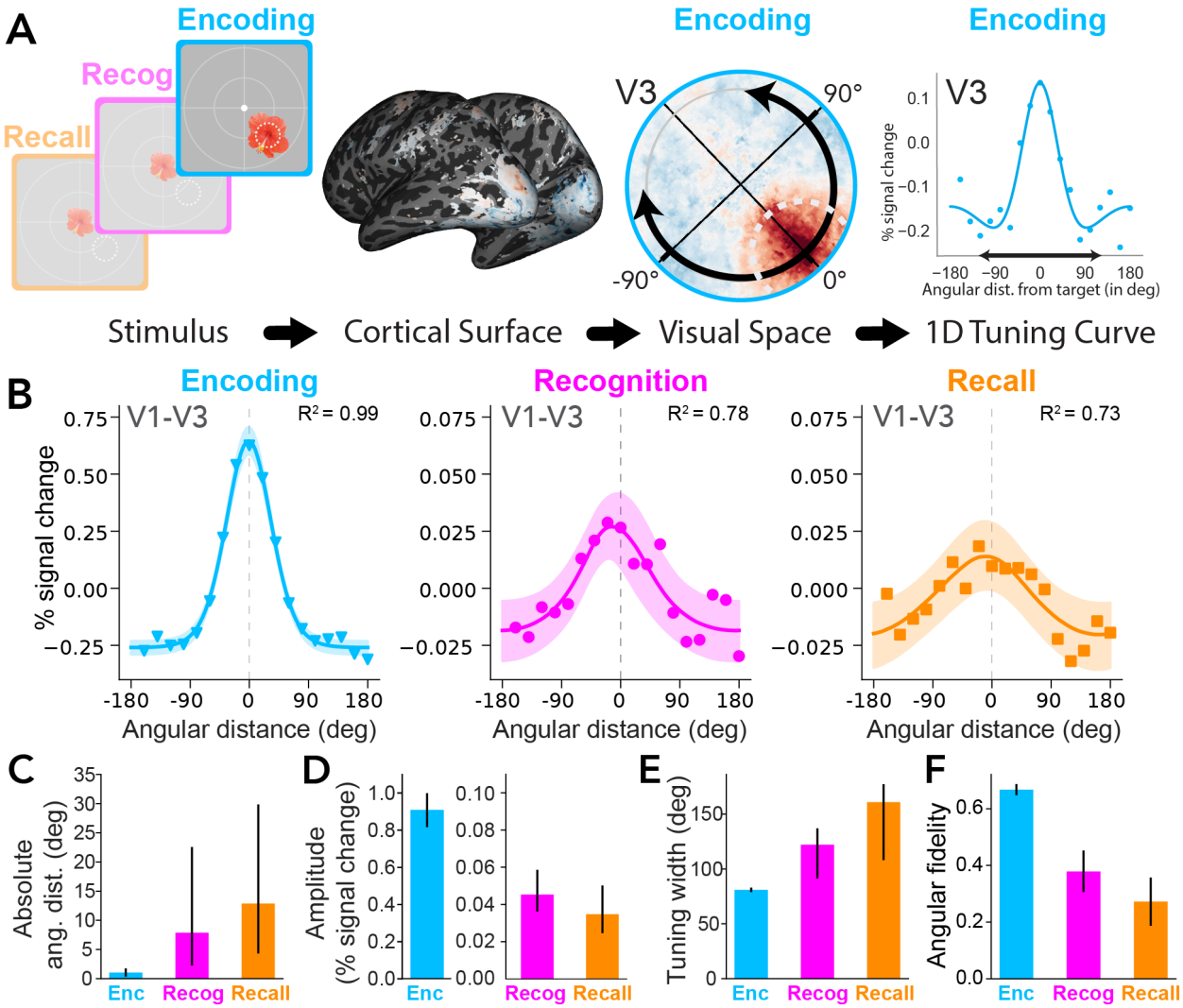

Figure 3. Single-shot memory responses in visual cortex are tuned to encoded location.

A) Mapping BOLD responses to polar angle activation profiles. A stimulus evokes a BOLD response in visual cortex. This activity is mapped to visual space and binned by angular distance from target, producing a tuning curve, here capturing the polar angle activation profile from the encoding task. This method is used to compare responses across encoding, recognition, and spatial recall tasks. B) Polar angle activation profiles fit to brain activity in early visual cortex (V1-V3). Shaded region indicates 68% confidence interval across subjects. While the spatial tuning of responses at encoding were predictably good, the responses during both retrieval tasks were also tuned to the studied object location, even though the object was only shown at that location once. C-F) Estimates of tuning quality observed during single-trial encoding, recognition, and recall. Error bars indicate 68% bootstrapped confidence intervals across subjects. C) Absolute distance between peak location and object source location. Responses at retrieval were less accurate than responses at encoding, but were still well aligned to the object's source location. D) The amplitude (peak to trough) of responses at retrieval were less than a tenth of those at encoding, yet still reliably above zero. E) The tuning width of responses at memory retrieval were characteristically broader than at encoding, consistent with previous studies. F) The memory responses, while having lower angular fidelity than the encoding response, also showed reliable fidelity.

For each task, we found that the center of the polar angle activation profiles was close to 0° away from the target location, indicating that activity in V1-V3 was spatially tuned to the object's polar angle location at encoding. The average distance between the activation profile and the stimulus location during encoding trials was 1° [95% CI 0°, 2°], during recognition 8° [0°, 31°] and during recall 12° [1°, 48°] (Figure 3B). The activation profiles for the encoding data were very well fit by the von Mises functions, with R^2 of 0.99. The memory data were not as well fit, but the von Mises functions still accounted for most of the variance: recognition R^2 of 0.78, recall R^2 of 0.73. The fact that the memory tasks produced tuned activity that clearly peaked near the encoded location (0°) confirms our hypothesis that a single encoding event is sufficient to produce spatially tuned responses in early visual cortex during memory retrieval. Tuned responses were observed during both recall and recognition tasks, even though location was not explicitly relevant for the recognition judgment.

We next quantified how the spatial tuning parameters of the memory retrieval responses compared to those from encoding. First, we compared the estimates of peak location reported above: we found that, compared to the encoding response, which peaked about 1° away from the object's location, the memory response peaked 7° [95 CI -1°, 30°] further during recognition and 12° [-1°, 47°] further during recall (Figure 3C). Second, the encoding response was 0.86% signal change [95 CI 0.71%, 1.03%] larger in amplitude than the recognition response, and 0.87% [0.72, 1.03] larger than the recall response (Figure 3D). In terms of ratio, the memory response amplitudes were about 25 times lower than perception (0.9 vs 0.035). Lastly, the responses during both memory retrieval tasks were more broadly tuned than those at encoding. The width of the encoding response (full width at half max) was 81° [68 CI 79°, 83°], the recognition was 122°, [68 CI 96°, 136°], and the recall response was 161° [68 CI 112°, 177°] (Figure 3E). While the broader tuning in early visual cortex during memory is consistent with our previous work, the amplitude of the memory responses here are a much smaller fraction of the perceptually evoked response than previously reported (Favila et al., 2022; Woodry et al., 2025).

We summarized the degree to which the tuning peaked at the target location by calculating the "fidelity" of each polar angle activation profile, in line with prior related work (Vo et al., 2022). Here, fidelity is a measure of the tuning quality of the response: the normalized length of the vector sum of the polar angle histogram projected to 0°. Fidelity ranges from -1 to +1, with a value of +1 when the BOLD amplitude is 0 in every bin except the one centered at 0°, a value of -1 when the amplitude is 0 everywhere except the bin at -180°, and 0 when the there is no directional bias toward 0° or 180°. This measure is a useful summary as it is influenced by several factors: fidelity is high when the center position is close to 0°, when the tuning is narrow, and when the data have low noise. The encoding response had a fidelity of 0.67 [95% CI 0.63, 0.71]. Both memory responses also showed good fidelity: recognition at 0.38 [0.19, 0.51] and recall at 0.32 [0.1, 0.44] (Figure 3F). The fidelity

measurements confirm the observations that there is reliable tuning in both memory tasks, and that the tuning is weaker in memory than in perception. Though we performed all of these analyses by pooling the data across visual field maps V1 to V3 for a higher signal-to-noise ratio, tuning is also evident in each separate area in all three tasks (supplementary Figure 3-1).

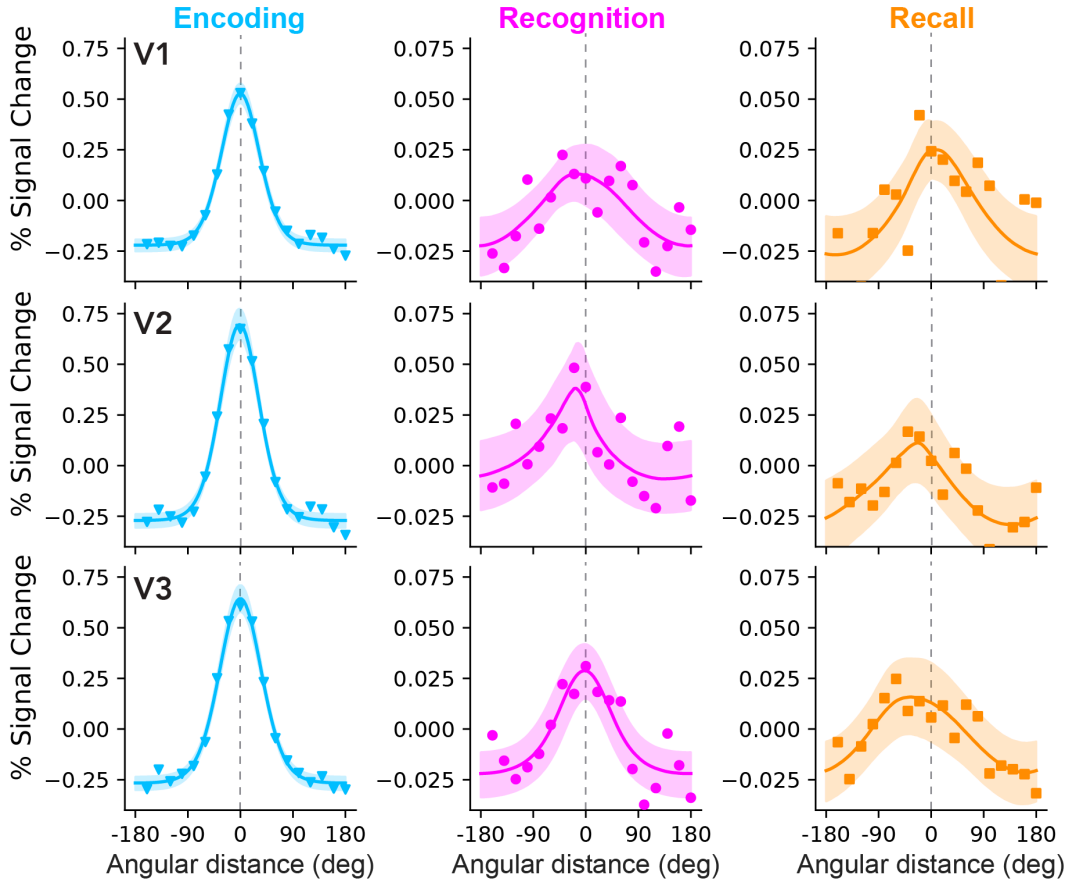

Supplemental Figure 3-1. Spatial tuning during encoding and retrieval for V1, V2, and V3

Polar angle activation profiles during encoding (blue), recognition (pink), and recall (orange) for each visual map V1, V2, and V3. The fidelity of the encoding and memory responses remained broadly consistent within individual visual maps. V1 encoding fidelity was at 0.65 [95% CI 0.58, 0.74], recognition was 0.31 [0.1, 0.42], and spatial recall was 0.26 [0.13, 0.33]. V2 encoding fidelity was at 0.63 [0.6, 0.68], recognition was 0.27 [-0.05, 0.48], and recall was 0.17 [-0.05, 0.4]. V3 encoding fidelity was at 0.71 [0.63, 0.73], recognition was 0.35 [0.14, 0.5], and recall was 0.32 [0.1, 0.41].

The group-averaged data reported above also hold at the individual subject level. We averaged across participants for the main analyses above because the signal-to-noise ratio of the BOLD response for individual subjects is relatively low in the memory conditions. Nonetheless, the overall patterns are evident in most of the individuals (supplementary Figure 3-2). To quantify tuning, we computed the fidelity summary metric for each participant in each condition. Fidelity was positive (indicating tuning) in all three conditions, with an average value of 0.6 [95% CI 0.57, 0.63] in encoding, 0.19 [0.1, 0.26] in recognition memory, and 0.15 [0.07, 0.22] in recall. To further quantify each participant's tuning, we compared their measured fidelity to the fidelity derived from a null distribution of fidelity values. The null distribution was

computed separately for each subject by scrambling the assignment of target locations across trials, and then re-computing the fidelity. This was done 1,000 times per participant. The fidelity measure was more than 2 sd greater than the mean fidelity of the null distribution for all 19 participants in the encoding condition, 14 of 19 in recognition memory, and 13 of 19 in recall. Overall, the individual participant analyses indicate that spatial tuning in visual cortex during memory was not an artifact of averaging across participants, but was instead evident in most individuals.

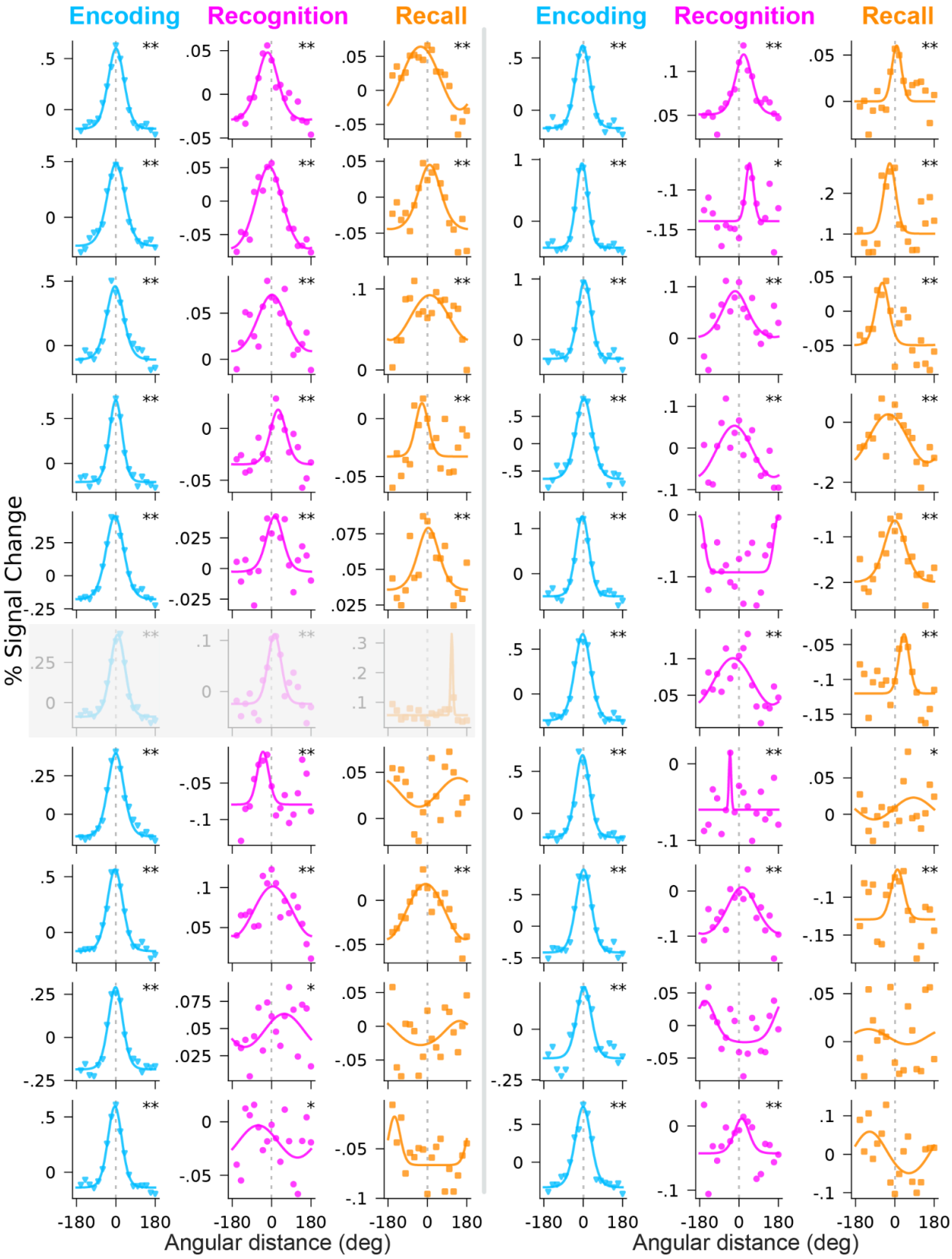
Encoding
Recognition
Recall
Encoding
Recognition
Recall
% Signal Change
Angular distance (deg)
Angular distance (deg)

Supplemental Figure 3-2. Spatial tuning during encoding and retrieval for individual subjects.
V1-V3 polar angle activation profiles for all subjects (n=20) and tasks. Transparent gray overlay indicates the subject excluded from group-level analyses due to not following response report instructions during the spatial recall memory task. Dashed grey lines indicate the original polar angle location of object. ** denotes responses with angular fidelity greater than 2 sd from the mean of the null distribution (generated for each subject and task), * denotes greater than 1 sd. The encoding responses are well tuned for all subjects. The memory responses are tuned for the majority of subjects.

Memory responses in early visual cortex track locations of remembered objects

To test if the presence of spatially tuned memory responses in visual cortex predicts successful recall, we grouped trials in each memory task by whether the object's location was later remembered or forgotten (behavioral report during spatial location recall, Figure 4A) and recomputed the polar angle activation profile for each group (Figure 4B). These profiles reveal clear spatial tuning, during both recognition and recall, when the object's location was successfully remembered. By contrast, the memory response was less tuned for trials where the object's location was forgotten, particularly during the recall task. Indeed, the fidelity of the recognition memory response dropped from 0.42 [95% CI 0.14, 0.56] for remembered trials to 0.16 [0.02, 0.36] for forgotten trials, while the fidelity of the spatial recall response dropped from 0.39 [0.17, 0.49] to 0.06 [-0.25, 0.26]. Specifically, the peak of the memory response was further from the target location for trials where the object location was forgotten compared to when the location was remembered. The recall response for forgotten trials peaked 89° [21°, 174°] further away from the target than the response for remembered trials (Figure 4C Right). While the von Mises fit to the recognition response for forgotten trials appears to indicate some tuning, we found that it peaked 50° [95 CI -8°, 106°] further away from the target (Figure 4C Left). Therefore, the tuning quality for the recognition memory response decreased substantially for forgotten trials. These effects are particularly evident in V1 (see supplementary Figure 4-1). These results reveal that accurate spatial tuning of memory responses in early visual cortex is associated with accurate spatial recall.

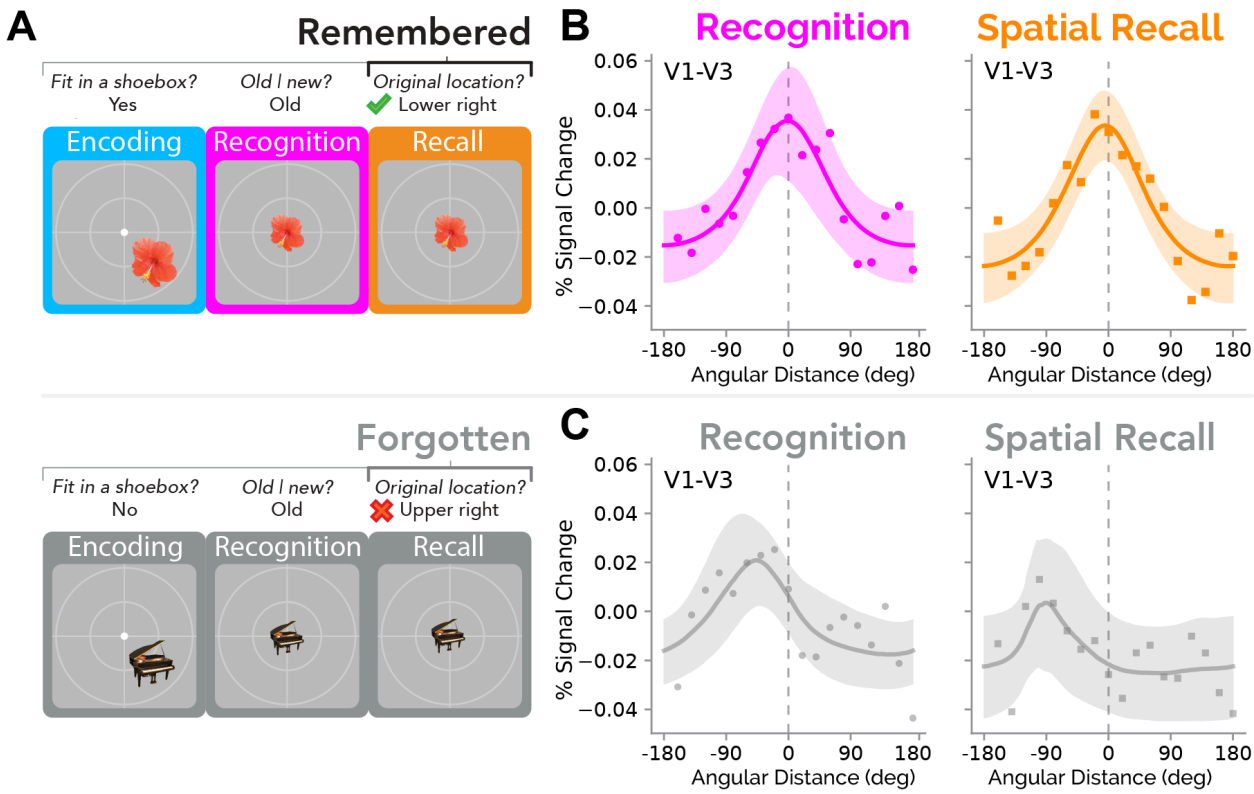

Figure 4. Spatially-tuned memory responses in early visual cortex track recall success

A) Schematic for grouping remembered/forgotten trials across tasks. Trials in each task (encoding, recognition, and recall) are assigned to the 'remembered' group if the object's location is reported correctly during the spatial recall task. Trials are deemed 'forgotten' if location is reported incorrectly during the recall task. B) Polar angle activation profiles fit to brain activity in early visual cortex during both memory tasks, for trials where the object's location was remembered at recall. C) Polar angle activation profiles fit to brain activity in early visual cortex during both memory tasks, for trials where the object's location was forgotten at recall. There is clearer tuning to the object's source location for remembered trials, especially for the recall task.

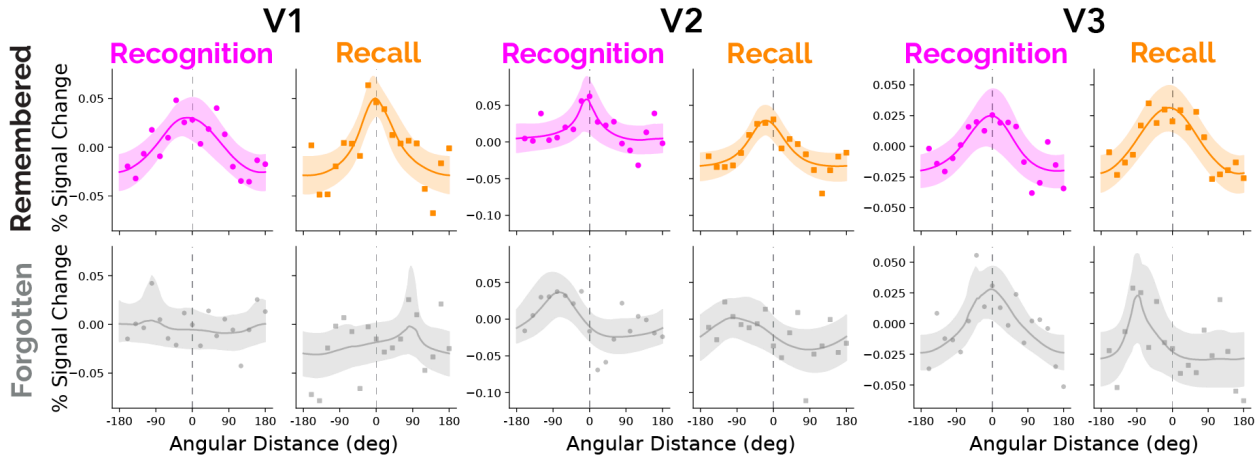

Supplemental Figure 4-1. Memory responses for remembered vs. forgotten trials in V1, V2, and V3

Polar angle activation profiles fit to brain activity in V1, V2, and V3 during both memory tasks. Trials are grouped according to whether an object's location was successfully remembered (pink and orange, top row) or forgotten (gray, bottom row) during the recall task. Tuning quality is robust across each visual map during both memory tasks when object location is remembered. Tuning quality drops when the object's location is forgotten. The drop in fidelity between remembered and forgotten trials is most evident in V1, where recognition fidelity drops from 0.39 [95% CI 0.11, 0.45] to -0.04 [-0.28, 0.22], and recall fidelity from 0.26 [0.13, 0.33] to 0.07 [-0.06, 0.17]. The decrease is less pronounced in V2, where recognition fidelity drops from 0.17 [-0.14, 0.40] to -0.02 [-0.15, 0.34], and recall fidelity from 0.24 [0.04, 0.52] to 0.01 [-0.27, 0.13]. In V3, while there is a large decrease in recall fidelity from 0.46 [0.15, 0.46] to 0.09 [-0.16, 0.27], there is almost no change in recognition fidelity from 0.30 [0.03, 0.53] to 0.26 [0.09, 0.37].

Still, it's possible that there are spatially tuned responses for forgotten trials, but not at the encoded location. If participants were either retrieving an incorrect memory or guessing and then attending to the reported location, we might expect tuning to the reported location but not the correct location. To address this possibility, we repeated the prior analyses but aligned population responses to the reported location. The fidelity of the forgotten memory response remained consistently poor across early visual cortex during both recognition and spatial recall: V1-V3 recognition fidelity was 0.14 [-0.06, 0.3] and recall was 0.03 [-0.24, 0.27]; V1 recognition fidelity was .05 [-0.1, 0.18] and recall was .07 [-0.28, 0.26]; V2 recognition fidelity was 0.07 [-0.12, 0.21] and recall was 0.02 [-0.13, 0.3]; V3 recognition fidelity was 0.24 [-0.01, 0.32] and recall was -0.22 [-0.35, 0.15] (see supplementary Figure 4-2). That the report-aligned spatial recall data were not tuned on forgotten trials suggests that the act of reporting the location is not responsible for the tuning during remembered trials.

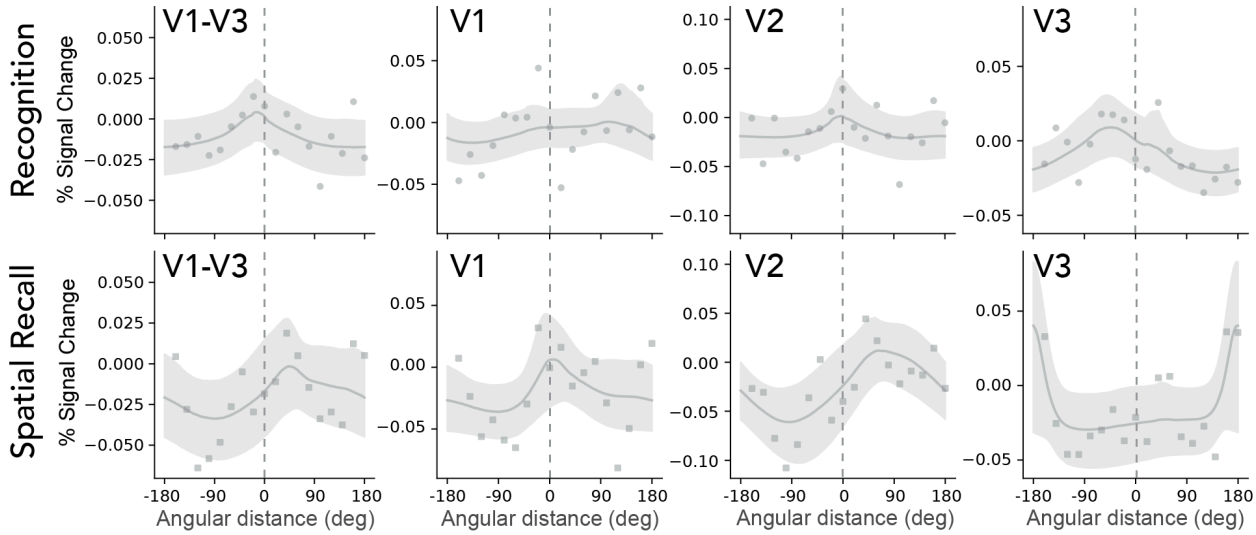

Supplemental Figure 4-2. Report-aligned memory responses for forgotten trials for all ROIs
Report-aligned polar angle activation profiles fit to brain activity in V1-V3 and each individual visual map during both memory tasks for trials where the object's location was forgotten. The tuning of the memory response for forgotten trials was consistently poor across all visual ROIs, even when the response on each trial was aligned to the behavioral report.

Spatial tuning at encoding predicts subsequent memory

Objects whose locations were remembered during the recall task may differ in how they were encoded, reflected by differences in cortical activity during stimulus presentation. This is typically referred to as a "subsequent memory effect". Previous research has generally failed to observe this subsequent memory effect in early visual cortex (Kim, 2011). However, prior studies tended to average visual cortex responses across maps, and subsequent memory effects might be limited to subpopulations of visual cortex. Our polar angle activation profiles provide a more precise way to quantify subsequent memory effects.

We tested for subsequent memory effects in visual cortex by comparing the spatial tuning profiles from the encoding task for subsequently remembered vs subsequently forgotten trials (Figure 5A). From these initial comparisons we found larger responses during encoding in each visual area for trials whose object locations were later remembered than for those later forgotten. Specifically, we found the amplitude (peak minus trough) of remembered trials was 0.11% signal change [95 CI 0.01, 0.21] larger than forgotten trials in early visual cortex (Figure 5B). Additionally, we found that this subsequent memory effect is spatially selective: by taking the difference of polar angle activation profiles between remembered and forgotten trials, we observe a gain in the response localized near the retinotopic location of the encoded object (Figure 5C), which is particularly evident in V3 (see supplementary Figure 5-1). Thus, a larger response in visual cortex during encoding is predictive of subsequent memory.

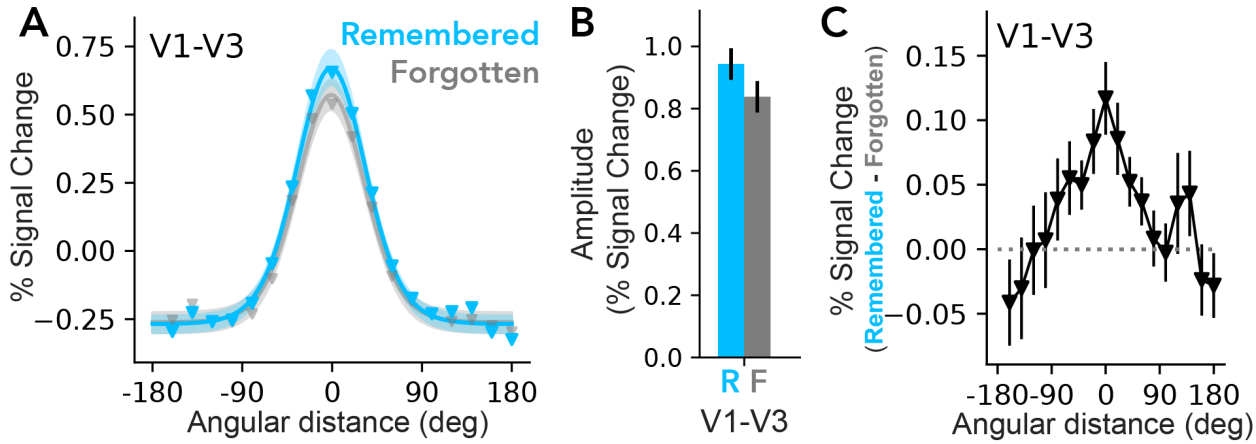

Figure 5. Spatial tuning in early visual cortex at encoding predicts subsequent recall

A) Polar angle activation profiles fit to brain activity from early visual cortex during encoding, grouped by whether the encoded object's location was later remembered (blue) or forgotten (gray) during the spatial recall task. Shaded region indicates 68% confidence interval across subjects. B) Amplitude estimates (peak to trough) during encoding for remembered and forgotten groups. Error bars indicate one standard deviation of the amplitude difference between the two groups across bootstraps. C) Differences in BOLD response between remembered and forgotten groups as a function of angular distance to the target. Error bars indicate one standard deviation of the bootstrapped differences between the two groups.

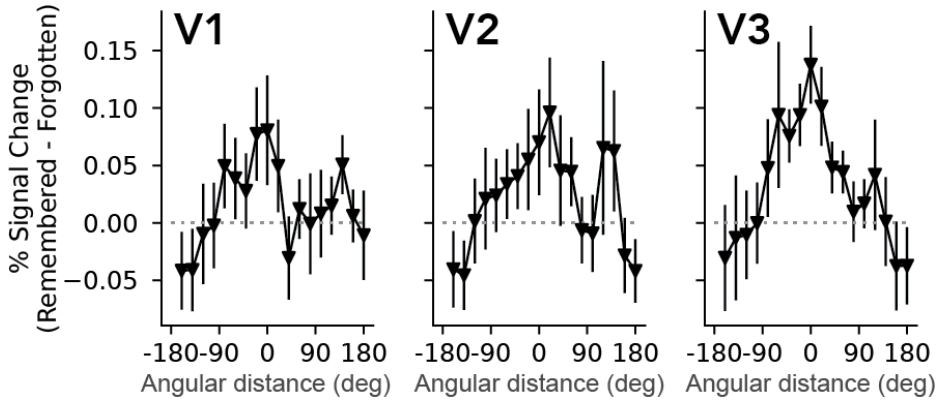

Supplemental Figure 5-1. Subsequent memory effect in V1, V2, and V3

Differences in BOLD response between remembered and forgotten trials as a function of angular distance to the target, for each visual map V1, V2, and V3. Error bars indicate one standard deviation of the bootstrapped differences between the two groups. The dashed grey line indicates equality between groups. V3 shows the largest difference between remembered and forgotten responses during encoding, smallest difference in V1.

Discussion

Summary

We measured the spatial tuning of visual cortical responses during encoding, recognition, and recall of visually presented objects in a one-shot encoding experiment. We demonstrated that a single encoding experience was sufficient to observe spatially tuned responses in early visual cortex during later memory retrieval. These responses occurred even when spatial information was not explicitly probed, indicating that such responses can arise spontaneously. However, the response amplitude in visual cortex due to memory was several times lower than what has been found in similar studies with more training prior to recall.

Despite the low amplitude of the memory responses, we found multiple relationships between visual cortex activity and memory behavior. First, location memory was associated with spatially tuned responses in visual cortex during both recognition and recall. Second, location memory was associated with spatial tuning during encoding – specifically, enhanced responses near the object location and reduced responses elsewhere. These results point to a strong link between the fidelity of early visual cortical representations and one-shot episodic memory performance. They also demonstrate that the engagement of early sensory areas during memory retrieval does not require highly-trained associations, a common component of lab studies, but rather is a generalizable property of episodic memory.

The role of early visual cortex in cognition

Whether early visual cortex plays a large role in memory and other cognitive tasks has been an important question for understanding how cortex functions. Feedback connections are as common as feedforward connections (Markov et al., 2014), and yet many influential models of cortex emphasize feedforward pathways. In particular, early models of visual cortex (Hubel & Wiesel, 1965; Marr, 2010) proposed that perception is accomplished by a chain of feedforward stages in a hierarchy, suggesting little role for early cortical areas in high level processes such as recognition or memory. The role of feedback projections in this view would be limited to modulatory signals rather than directly triggering responses, as in the "no strong loops hypothesis" (Crick & Koch, 1998). Hence early visual areas would not routinely participate in memory-related processes. Rather, top-down effects would only be observed for highly practiced tasks or when top-down demands are very high, as in imagery of fine spatial details or precise deployment of spatial attention. This view is supported by consistent findings of overlapping activity during perception and memory/imagery in higher level visual areas, but more variable evidence in early visual cortex (Kosslyn & Thompson, 2003), and by the finding that attentional effects are small in early visual cortex compared to more anterior visual areas (Crick & Koch, 1998; Maunsell & Cook, 2002; Yoshor et al., 2007).

Some more recent theories propose that because primary sensory areas like V1 have circuitry well suited for detailed, high-resolution analysis, they serve as a buffer, or "blackboard", for analyzing images via feedback processes (Gilbert & Sigman, 2007; Lee et al., 1998; Lee & Mumford, 2003; Williams et al., 2008). Consistent with the latter view, memory studies have shown that early visual cortex carries stimulus information during retrieval: low-level features (such as orientation or spatial location) can be recovered from V1 to V3 activity patterns using decoding methods (Bone & Buchsbaum, 2021; Bosch et al., 2014; Vo et al., 2022) or encoding models (Breedlove et al., 2020; Favila et al., 2022; Favila & Aly, 2023; Woodry et al., 2025).

Our findings help to clarify the two views. On the one hand, we show clear evidence that V1–V3 contains mnemonic signals that carry stimulus information and predict recall success. This pattern of data is broadly consistent with prior studies that have linked decoded memory content to recall behavior (Gordon et al., 2014; Kuhl et al., 2011; Polyn et al., 2005). Moreover, we see spatially tuned memory responses even when task demands do not explicitly encourage it, and even when an item was only encountered once before, without the need for explicit imagery or repeated practice. These findings dovetail with other recent work suggesting an automatic involvement of sensory systems in internally-oriented cognition (Zokaei et al., 2019). On the other hand, these mnemonic signals were about 20 times lower in amplitude than their visually-evoked counterparts. A virtue of low amplitude signals is that they likely enable cortex to continue to faithfully signal incoming sensory information even during cognitive acts. Taken together, these findings suggest that early visual cortex, while predominantly playing a major role in bottom-up processing of sensory information, also plays a supportive role in top-down processing of cognitive information.

While our results clearly demonstrate that early visual cortex contains mnemonic representations, and that these representations relate to behavioral outcomes, we do not interpret this as evidence that long-term memories are stored in early visual areas themselves. Although local plasticity in early visual cortex can support some forms of cognition like iconic memory (Teeuwen et al., 2021), perceptual learning (Jehee et al., 2012), and adaptation (Gardner et al., 2005), such mechanisms are unlikely to account for the effects observed in the current study. Iconic memory and adaptation tend to occur on short timescales and perceptual learning requires substantial repetition. Our paradigm involved no repetition or training and tested memory for single events after a delay of several minutes with many intervening images. The timescale of the observed effects instead suggests that mnemonic responses in early visual cortex likely depend on storage in other brain areas. The hippocampus, which has circuitry that is specialized for rapid plasticity and which is necessary to encode new memories, is the most likely candidate region (Knierim, 2015).

Low amplitude responses during recall of one-shot memories

The amplitudes of the memory responses we observed here were lower relative to the stimulus evoked responses than what we found in prior studies (Favila et al., 2022; Woodry et al., 2025)). In those studies, the memory signals were only four times lower than perceptual signals, compared to 25-fold here. The substantial decrease in the relative strength of the memory response here is consistent with the idea that repeated study and retrieval practice increase the strength of the memory response in early visual cortex. Despite the low amplitude of V1 to V3 memory responses, we still observed precisely tuned memory responses predictive of recall behavior. The relatively low amplitude modulations of early sensory cortex observed here may be more typical of top-down effects than those found when participants are highly practiced at a particular memory.

The encoding model we used facilitated detection and quantification of memory responses in early visual cortex. Indeed, had we not assessed these responses through the lens of an encoding model, we likely would have missed the spatially tuned responses. This is because, first, the amplitudes were low and there is considerable noise in the trial to trial responses, hence a typical decoding model would be underpowered. Second, the tuning curves shift depending on stimulus location at encoding, hence univariate analyses that averaged the V1 response across trials would blur out the signal.

Incidental reactivation in early visual cortex

Strikingly, we observed spatially tuned responses in early visual cortex in the recognition task, when spatial location was not relevant. This indicates that reactivation of perceptual representations can occur in the absence of explicit retrieval demands for spatial information. Why should the brain generate irrelevant signals? One plausible explanation is that retrieval initially reactivates all or many of the features of a memory irrespective of the task demand, after which higher level cortical regions then extract the information relevant for a particular task (Favila et al., 2018; Kuhl et al., 2013; Kwak & Curtis, 2022). Generating only the cortical responses that are task-relevant would require finer and more flexible top-down control. An alternative possibility is that participants in our experiment knew that they would be tested on object locations, and thus may have been strategically recalling spatial information during the recognition task in order to practice for the recall task. Spatial tuning in the recognition task, then, could in part be caused by spatial recall. Regardless of whether spatial tuning during recognition reflects strategic covert recall or is spontaneous, our results support the idea that spatial tuning is related to successful memory retrieval and not to other response-related variables. When we aligned memory responses to the reported location for 'forgotten' trials, we failed to find tuning present in the recognition and recall responses. This suggests that the spatially tuned memory response in early visual cortex is not caused by the decision (commitment to one of the choices) or the response (button press), but is more likely associated with memory of the location.

Subsequent memory effects

Interestingly, we found that tuning differences related to successful memory were evident at encoding: subsequently remembered items elicited stronger responses near the object's location and weaker responses elsewhere compared to subsequently forgotten items. Notably, prior work on subsequent memory effects has not typically implicated early visual cortex (Kim, 2011). Such responses might have been missed since most papers on subsequent memory look for univariate differences across entire regions of interest. Here, we see small, but robust, subsequent memory effects at specific visual field locations which change on each trial, and which would be obscured by averaging over all of early visual cortex. The spatial specificity of these effects suggests that they are unlikely to be caused by global mechanisms like arousal, which would impact the entire visual field map (Burlingham et al., 2022).

There are several plausible mechanisms that could yield localized gains in the early visual cortex response for subsequently remembered items. First, these effects could be caused by stimulus properties such as image memorability (Rust & Mehrpour, 2020). Image memorability effects differ from subsequent memory effects in that their neural correlates are independent of whether an individual subject remembers the image or not (Bainbridge et al., 2017; Mohsenzadeh et al., 2019). Enhanced responses related to image memorability have thus far only been reported in higher level visual cortex and the medial temporal lobe, and have not been reported in early visual cortex (Bainbridge et al., 2017; Bainbridge & Rissman, 2018). Another candidate mechanism is fluctuations in spatial attention. Attention is known to enhance the neural representation of relevant information in visual cortex (Tootell et al., 1998; Uncapher & Rugg, 2009). Participants likely attended to the location of the target during encoding, and there would naturally be trial-to-trial variation in the level of attention deployed. While we did not have a behavioral measure of attention, limiting our ability to draw strong conclusions about it here, there are several reasons to favor this interpretation. First, selective attention is known to modulate activity in early visual cortex in a similar manner to what we observed (Ling et al., 2015; Tootell et al., 1998; Tünçok et al., 2024). Second, attention has been repeatedly implicated in promoting memory encoding (Craik et al., 1996; Uncapher & Wagner, 2009; Wager et al., 2004).

Conclusion

Collectively, this work makes significant progress on characterizing memory reactivation in human cortex by using a one-shot encoding paradigm that echoes the demands of real world episodic memory. We demonstrate an important role for early visual cortex in promoting the successful encoding and retrieval of sensory details from once-experienced events.

Materials and Methods

Subjects

20 human subjects (12 females, 25-47 years old) were recruited to participate in the experiment and were compensated for their time. One participant was excluded from the analysis because they misunderstood the instructions for providing behavioral responses during the spatial recall task. An initial group of 5 subjects were used for pilot analyses while the remaining 14 were used to validate those analyses. We report here the analyses across all 19 subjects. Subjects were recruited from the New York University community and included the authors S.E.F. and J.W. Subjects other than the authors were naive to the study's purpose. All subjects gave written informed consent to procedures approved by the New York University Institutional Review Board prior to participation. All subjects had no MRI contraindications, normal color vision, and normal or corrected-to-normal visual acuity.

Stimuli

Object stimuli

This experiment involved testing memory retrieval after a single encoding experience. Therefore, this required the use of a large number of easily recognizable cues with a low probability of confusion. Based on subjective ratings from six subjects not included in the pilot or main experiment, we identified 480 everyday object images from a publicly available dataset that were recognizable in the near periphery (BOSS dataset, (Brodeur et al., 2010). For each set of the three tasks (encoding, recognition, location), 48 small images of unique objects were sampled without replacement from the 480 images. This produced ten non-overlapping subsets of images — one for each set of three tasks. Within each subset, half (24) were randomly selected without replacement to be used in both the encoding and location tasks, while the total (48) were used in the recognition task.

On each trial, a small image of one of these objects was shown in either the near periphery (for encoding trials) or at fixation (for recognition and location trials). During the encoding task, objects were presented at one of four equispaced peripheral locations around the visual field (45°, 135°, 225°, and 315°) at 2° eccentricity from a central fixation point, spanning 2.5° of visual angle. For the recognition and location tasks, objects were presented at fixation, spanning 1.5° visual angle.

A circular guide spanned the visual field, centered at fixation. This guide consisted of three concentric white circles increasing in radii (2°, 4°, and 6° eccentricity), a horizontal and vertical line that each bisected the circles, and a small white dot at fixation. Object stimuli were presented on top of this guide to provide an external spatial frame of reference.

Experimental Procedure

The experiment cycled through sets of three scans: encoding, recognition, location. These sets were repeated five times per scan session (Figure 1). Each subject participated in two scan sessions, for a total of 30 scans (10 per task). encoding and location scans consisted of 24 trials, one for each object, in random order. Recognition scans consisted of 48 trials, one for each object from the prior encoding task (old), and another 24 objects not seen before in the experiment (new) — all in random order. Objects in the encoding task were randomly assigned to, and presented in one of, four peripheral locations. This resulted in a total of 240 trials each for encoding and location tasks, and 480 trials for recognition tasks, across both scan sessions. Behavioral responses on each trial were collected using a four-response button box. Subjects were instructed to maintain central fixation for all tasks. An EyeLink 1000 Plus eye tracker was used to collect gaze position data and ensure fixation. The eye tracker was mounted onto a rig in the magnet bore that holds the projection screen.

For each encoding trial, an object was presented in the periphery for 2 seconds. This was followed by an inter-trial interval lasting 4 to 7 seconds. Subjects were instructed to indicate whether the peripherally presented object was smaller than a shoebox (1), larger than a shoebox (2), or unrecognizable (3).

For each recognition trial, an old (from the prior encoding task) or new object was presented at fixation for 2 seconds. This was followed by an inter-trial interval lasting 4-7 seconds. Subjects were asked to indicate whether the centrally presented object was old (1), or new (2).

For each location trial, an old object (from the prior encoding task) was presented at fixation for 2 seconds. This was followed by an inter-trial interval lasting 4-7 seconds. Subjects were asked to indicate the object's original location from the prior encoding task (1: upper right, 2: lower right, 3: lower left, 4: upper left).

Retinotopic mapping procedure

Each participant additionally underwent 10-12 retinotopic mapping scans in a separate scan session. The stimuli and procedures for the retinotopic mapping session followed those used in Himmelberg et al. (2021), summarized briefly here. Each scan involved contrast patterns presented within bar apertures (1.5° width), which swept across the visual field within a 12°-radius circle. There were 8 bar sweep types in total, comprising 4 diagonal directions and 4 cardinal directions. Each bar sweep took 24s to complete: cardinal sweeps took 24 s to traverse the full extent of the circular aperture; diagonal sweeps took 12 seconds to move to the halfway point, subsequently followed by 12 second long blank periods. Each functional scan comprised 8 sweeps, for a total of 192 seconds. The contrast patterns featured pink noise (grayscale) backgrounds with randomly sized and placed items, updated at 3 Hz. Participants were instructed to press a button whenever the fixation dot changed color, which occurred

approximately once every three seconds. These contrast patterns were originally implemented by Benson et al. (2018).

MRI Acquisition

A 3T Siemens Prisma MRI system and a Siemens 64-channel head/neck coil was used to collect functional and anatomical images at the Center for Brain Imaging at New York University. We obtained functional images using a T2*-weighted multiband echo planar imaging (EPI) sequence with whole-brain coverage (repetition time = 1 s, echo time = 37 ms, flip angle = 68°, 66 slices, 2 x 2 x 2 mm voxels, multiband acceleration factor = 6, phase-encoding = posterior-anterior). To estimate and correct susceptibility-induced distortions in the functional EPIs, we collected spin echo images with both anterior-posterior and posterior-anterior phase-encoding. Additionally, for each of the 20 subjects, we acquired one to three whole-brain T1-weighted MPRAGE 3D anatomical volumes (.8 x .8 x .8 mm voxels).

MRI Processing

We used *pydeface* (https://github.com/poldracklab/pydeface) to deface and anonymize all original MRI data (DICOM files). We then used the Heuristic Dicom Converter (Halchenko et al., 2018) to convert this data to NIFTI and organized the files into the Brain Imaging Data Structure format (K. J. Gorgolewski et al., 2016). We then preprocessed the data using fMRIPrep 20.2.7 (Esteban et al., 2018, 2019), which is based on Nipype 1.7.0 (K. Gorgolewski et al., 2011; K. J. Gorgolewski et al., 2018).

Anatomical data preprocessing.

The following sections on anatomical and functional data preprocessing are provided by the fMRIPrep boilerplate text generated by the preprocessed scan output.

Each of the one to three T1w images was corrected for intensity non-uniformity with N4BiasFieldCorrection (Tustison et al., 2010), distributed with ANTs 2.3.3 (Avants et al., 2008). The T1w-reference was then skull-stripped with a Nipype implementation of the antsBrainExtraction.sh workflow (from ANTs), using OASIS30ANTs as target template. Brain tissue segmentation of cerebrospinal fluid, white-matter and gray-matter was performed on the brain-extracted T1w using fast (FSL 5.0.9, (Zhang et al., 2001)). A T1w-reference map was computed after registration of the T1w images (after intensity non-uniformity-correction) using mri_robust_template (FreeSurfer 6.0.1, (Reuter et al., 2010)). Brain surfaces were reconstructed using recon-all (FreeSurfer 6.0.1, (Dale et al., 1999)), and the brain mask estimated previously was refined with a custom variation of the method to reconcile ANTs-derived and FreeSurfer-derived segmentations of the cortical gray-matter of Mindboggle (Klein, 2017).

Functional data preprocessing.

For each of the 30 BOLD runs found per subject (across all tasks and sessions), the following preprocessing was performed. First, a reference volume and its skull-stripped version were generated by aligning and averaging a single-band reference. A B0-nonuniformity map (or

fieldmap) was estimated based on two EPI references with opposing phase-encoding directions, with 3dQwarp (Cox & Hyde, 1997). Based on the estimated susceptibility distortion, a corrected EPI reference was calculated for a more accurate co-registration with the anatomical reference. The BOLD reference was then co-registered to the T1w reference using bbregister (FreeSurfer) which implements boundary-based registration (Greve & Fischl, 2009). Co-registration was configured with six degrees of freedom. Head-motion parameters with respect to the BOLD reference (transformation matrices, and six corresponding rotation and translation parameters) are estimated before any spatiotemporal filtering using mcflirt (FSL 5.0.9, (Jenkinson et al., 2002)). BOLD runs were slice-time corrected to 0.445s (0.5 of slice acquisition range 0s-0.89s) using 3dTshift from AFNI 20160207 (Cox & Hyde, 1997). First, a reference volume and its skull-stripped version were generated using a custom methodology of fMRIPrep. The BOLD time-series were resampled onto the fsnative surface. The BOLD time-series (including slice-timing correction) were resampled onto their original, native space by applying a single, composite transform to correct for head-motion and susceptibility distortions. These resampled BOLD time-series will be referred to as preprocessed BOLD. All resamplings can be performed with a single interpolation step by composing all the pertinent transformations (i.e. head-motion transform matrices, susceptibility distortion correction, and co-registrations to anatomical and output spaces). Gridded (volumetric) resamplings were performed using antsApplyTransforms (ANTs), configured with Lanczos interpolation to minimize the smoothing effects of other kernels (Lanczos, 1964). Non-gridded (surface) resamplings were performed using mri_vol2surf (FreeSurfer).

Many internal operations of fMRIPrep use Nilearn 0.6.2 (Abraham et al., 2014), mostly within the functional processing workflow. For more details of the pipeline, see the section corresponding to workflows in fMRIPrep's documentation.

General linear models

From each subject's surface based time series, we used GLMSingle (Prince et al., 2022) to estimate the neural pattern of activity during the 2 second stimulus presentations for each trial. GLMsingle first fits to each vertex's time series an optimal response function from a bank of 20 candidate hemodynamic response functions (Natural Scenes Dataset, (Allen et al., 2021)). Second, noisy vertices from the are identified from the data(defined by negative R^2) and then used to estimate noise regressors. This step iteratively uses principal component analysis to derive the noise regressors, an optimal number of noise regressors is chosen and then projected out of the time series' data. Third, fractional ridge regression is used to improve the robustness of single-trial beta estimates, particularly useful here as our design relies on single-trial encoding, recognition, and retrieval of object stimuli.

We constructed three separate design matrices to model the BOLD time series using GLMSingle, one for each of the three tasks. Each of the three design matrices has a regressor

corresponding to the object's true location ('target-aligned'). Recognition design matrices had an additional regressor for 'new' objects.

Population receptive field models

Data from the retinotopy session were used to fit a population receptive (pRF) model to each vertex on the cortical surface, as described by Himmelberg et al. ((Himmelberg et al., 2021); section 2.6). To briefly summarize, we fit a circular 2D-Gaussian linear pRF to each surface vertex's BOLD time series, averaged across identical runs of the bar stimulus. These fits were implemented with *Vistasoft* software (Dumoulin & Wandell, 2008), in conjunction with a wrapper function to handle surface data (https://github.com/WinawerLab/prfVista). Gaussian center (*x, y*) and standard deviation (σ) comprised the pRF model parameters.

Visual field map definitions

We used the visual tool *cortex-annotate* (https://github.com/noahbenson/cortex-annotate), which is built on *neuropythy* software (Benson & Winawer, 2018), to draw and define visual field maps for each subject. To do so, we traced the polar angle reversals on each subject's cortical surface. We followed common heuristics to define four maps spanning early visual cortex: V1, V2, V3 (Benson et al., 2022; Himmelberg et al., 2021). We then defined experiment-specific regions of interest for each visual field map. To do this we excluded vertices whose variance explained was less than 10% and whose pRF centers were outside one σ of 2° (the target eccentricity in the experiments). For example, a vertex with a pRF center at 1° and pRF size (σ) of 0.5° would be excluded, but a vertex with pRF center at 3° and pRF size of 1.5° deg would be included. We restricted vertices in our analyses this way to examine polar angle activation profiles, described in the next section. These mapping estimates are solely based on the retinotopy scans, and are therefore independent of the main experiment.

Quantifying behavioral performance at recognition and recall

Object recognition

During the recognition task, subjects responded with either 'new' or 'old' for objects presented at fixation. Half of these objects were present in the previous encoding task ('old'), the rest 'new'. Hits were classified as trials where previously seen objects were correctly identified as 'old'. Misses were classified as trials where previously seen objects were incorrectly identified as 'new'. Correct rejections were classified as trials where new objects were correctly identified as 'new'. False alarms were classified as trials where new objects were incorrectly identified as 'old'. For each scan, the total number of hits were divided by the total number of 'old' objects, to get hit rate as a percentage. Likewise, the total number of false alarms was divided by the total number of 'new' objects to get the false alarm rate as a percentage. Miss and correct rejection rates were calculated as the complement of the hit and false alarm rates, respectively.

Spatial location recall

During the location task, subjects reported which of four locations the object presented at fixation originally appeared at (from the encoding task). Trials were classified as accurate or

inaccurate if the reported location matched that of the original location, or source location, of the object, respectively. Therefore, because all objects shown were 'old' objects that had appeared within the encoding task in one of four locations, the chance level was at 25%. For each scan, the total number of accurate responses were divided by the number of trials to get mean accuracy.

Analyses quantifying spatial tuning in visual cortex at encoding and retrieval

We computed polar-angle activation profiles for each task (encoding, recognition, location) across a region of interest comprising visual maps V1, V2, and V3. To do so, we first obtained response amplitudes from the outputs of GLMsingle for each vertex on the cortical surface and each trial. PRF mapping, which was conducted in a separate fMRI session, returned visual field coordinates for each vertex. We excluded vertices not included in the ROI definitions outlined above. We further restricted trials by several criteria: for all tasks, we only included trials where behavioral responses were provided. In the recognition task, we only included trials that were classified as 'hits' (subject reported 'old' when viewing an 'old' object). Some analyses further restricted trials across all tasks to those whose object locations were accurately reported in the recall task. We binned the response amplitudes for the remaining trials and vertices by the angular distance between each vertex's preferred polar angle and the source location for that object. This binning by angular distance allows for averaging trials across the four peripheral source locations. This produces an activation profile as a function of distance from the object's source location; an activation profile for each subject and task. Each activation profile is then normalized by dividing by the vector length of the perceptually evoked activation profile (from the encoding task) for the corresponding subject. We then preserved meaningful units by rescaling each activation profile by the average vector lengths from the encoding task. Each of the resulting averaged activation profiles peaked near 0°, where values decreased moving away from the peak response. We therefore fit a von Mises distribution to the averaged activations as a function of angular distance to the source location, θ_{source} (Eq. 1). From each of these fits we estimated the peak location, the amplitude (peak to trough), and the width (full-width-at-half-maximum; FWHM).

$$f(\theta_{source}|\mu, k, s) = s\frac{e^{kcos(\theta_{source}-\mu)}}{2\pi I_0(k)} \qquad \text{Eq. 1}$$

Each metric provides a quantitative measure of some aspect of the tuning. However, on their own they can not provide a holistic picture of the quality of the tuning; for example, the response may be narrow but peak at a location opposite the source. Therefore to summarize the degree to which the tuned response concentrates at the source location we computed an angular "fidelity" metric which normalizes the length of the vector sum of the polar angle activation profile projected to 0° — a modified version of the circular fidelity metric used in prior related work (Vo et al., 2022).

To compute this metric, we first baseline subtracted each polar angle activation profile to remove any negative values. We then defined each binned activation (w_j) to be a vector pointing in the direction of the bin location (α_j) with a length equal to the activation, and then summed all 18 component vectors. We normalized the resultant vector by dividing the summed length of all component vectors. The direction of the normalized resultant vector captures the circular mean of each activation profile (Eq. 2), and the resultant vector length captures how concentrated the activations are near the mean direction (Eq. 3). Both the circular mean and resultant vector length are metrics derived from the CircStats MATLAB toolbox (Berens, 2009). The fidelity metric is obtained by multiplying the cosine of the circular mean, which captures how far away the mean is from 0°, by the resultant vector length (Eq. 4). Because cosine goes from -1 to 1, and the resultant vector length is normalized to be between 0 and 1, the fidelity metric is bound between +1 and -1. A value of 1 indicates a BOLD amplitude of 0 in every bin except the one centered at 0° (maximum directional bias towards 0°), a value of -1 indicates an amplitude of 0 everywhere except the bin at 180° (maximum directional bias away from 0°), and a value of 0 indicates no directional bias.

$$circular\ mean(\alpha, w) = angle(\sum_{j=0}^{n} w_j\ e^{i\ \alpha_j}) \qquad \text{Eq. 2}$$

$$resultant\ vector\ length(\alpha, w) = \frac{abs(\sum_{j=0}^{n} w_j\ e^{i\ \alpha_j})}{\sum_{j=0}^{n} w_j} \qquad \text{Eq. 3}$$

$$fidelity(\alpha,\ w) = cos(circular\ mean(\alpha,\ w))\ *\ resultant\ vector\ length(\alpha,\ w) \qquad \text{Eq. 4}$$

We repeated the von Mises and fidelity analyses, bootstrapping across subjects with replacement 10,000 times to obtain 68% and 95% confidence intervals for each of these four tuning metrics.

Resampling statistics

We analyzed bootstrapped data to infer spatial tuning properties as a function of condition and of other trial-level factors. Statistics reported in this paper are derived from these bootstrapped analyses. We report the mean and confidence intervals (CI) obtained from these analyses to assess our main claims. We report the 95% CI (corresponding to ±2 standard deviations of a normal distribution) when drawing comparisons between a measurement and a fixed value. When comparing two estimates, we instead report the 68% CIs (corr. ±1 standard deviation).

Software

Model fitting, data visualization, and statistical quantification for all analyses described in this paper were made using matplotlib 3.5.2 (Hunter, 2007), nibabel 3.2.2 (Brett et al., 2022), pandas 1.4.2 (The pandas development team, 2024), scikit-learn 1.0.2 (Pedregosa et al., 2011),

scipy 1.8.0 (Virtanen et al., 2020), and seaborn 0.11.2 (Waskom, 2021). Functions to compute circular statistics were converted to python from the CircStats MATLAB toolbox (Berens, 2009).

Data Availability

The data and code used to reproduce the analyses in this paper can be found at https://osf.io/a9hkg/.

REFERENCES

Abraham, A., Pedregosa, F., Eickenberg, M., Gervais, P., Mueller, A., Kossaifi, J., Gramfort, A., Thirion, B., & Varoquaux, G. (2014). Machine learning for neuroimaging with scikit-learn. *Frontiers in Neuroinformatics*, *8*, 14.

Allen, E. J., St-Yves, G., Wu, Y., Breedlove, J. L., Prince, J. S., Dowdle, L. T., Nau, M., Caron, B., Pestilli, F., Charest, I., Hutchinson, J. B., Naselaris, T., & Kay, K. (2021). A massive 7T fMRI dataset to bridge cognitive neuroscience and artificial intelligence. *Nature Neuroscience*, *25*(1), 116–126.

Avants, B. B., Epstein, C. L., Grossman, M., & Gee, J. C. (2008). Symmetric diffeomorphic image registration with cross-correlation: evaluating automated labeling of elderly and neurodegenerative brain. *Medical Image Analysis*, *12*(1), 26–41.

Bainbridge, W. A., Dilks, D. D., & Oliva, A. (2017). Memorability: A stimulus-driven perceptual neural signature distinctive from memory. *NeuroImage*, *149*, 141–152.

Bainbridge, W. A., & Rissman, J. (2018). Dissociating neural markers of stimulus memorability and subjective recognition during episodic retrieval. *Scientific Reports*, *8*(1), 8679.

Benson, N. C., & Winawer, J. (2018). Bayesian analysis of retinotopic maps. *eLife*, *7*. https://doi.org/10.7554/eLife.40224

Benson, N. C., Yoon, J. M. D., Forenzo, D., Engel, S. A., Kay, K. N., & Winawer, J. (2022). Variability of the Surface Area of the V1, V2, and V3 Maps in a Large Sample of Human Observers. *The Journal of Neuroscience: The Official Journal of the Society for Neuroscience*, *42*(46), 8629–8646.

Berens, P. (2009). CircStat: AMATLABToolbox for Circular Statistics. *Journal of Statistical Software*, *31*(10), 1–21.

Bone, M. B., & Buchsbaum, B. R. (2021). Detailed episodic memory depends on concurrent

reactivation of basic visual features within the posterior hippocampus and early visual cortex. *Cerebral Cortex Communications*, *2*(3), tgab045.

Bosch, S. E., Jehee, J. F. M., Fernández, G., & Doeller, C. F. (2014). Reinstatement of associative memories in early visual cortex is signaled by the hippocampus. *The Journal of Neuroscience: The Official Journal of the Society for Neuroscience*, *34*(22), 7493–7500.

Breedlove, J. L., St-Yves, G., Olman, C. A., & Naselaris, T. (2020). Generative Feedback Explains Distinct Brain Activity Codes for Seen and Mental Images. *Current Biology: CB*, *30*(12), 2211–2224.e6.

Brett, M., Markiewicz, C. J., Hanke, M., Côté, M.-A., Cipollini, B., McCarthy, P., Jarecka, D., Cheng, C. P., Halchenko, Y. O., Cottaar, M., Larson, E., Ghosh, S., Wassermann, D., Gerhard, S., Lee, G. R., Wang, H.-T., Kastman, E., Kaczmarzyk, J., Guidotti, R., … freec84. (2022). nipy/nibabel: 3.2.2 (3.2.2). Zenodo. https://doi.org/10.5281/zenodo.6617121

Brodeur, M. B., Dionne-Dostie, E., Montreuil, T., & Lepage, M. (2010). The Bank of Standardized Stimuli (BOSS), a new set of 480 normative photos of objects to be used as visual stimuli in cognitive research. *PloS One*, *5*(5), e10773.

Burlingham, C. S., Ryoo, M., Roth, Z. N., Mirbagheri, S., Heeger, D. J., & Merriam, E. P. (2022). Task-related hemodynamic responses in human early visual cortex are modulated by task difficulty and behavioral performance. *eLife*, *11*, e73018.

Cox, R. W., & Hyde, J. S. (1997). Software tools for analysis and visualization of fMRI data. *NMR in Biomedicine*, *10*(4-5), 171–178.

Craik, F. I., Govoni, R., Naveh-Benjamin, M., & Anderson, N. D. (1996). The effects of divided attention on encoding and retrieval processes in human memory. *Journal of Experimental Psychology. General*, *125*(2), 159–180.

Crick, F., & Koch, C. (1998). Constraints on cortical and thalamic projections: the no-strong-loops hypothesis. *Nature*, *391*(6664), 245–250.

Dale, A. M., Fischl, B., & Sereno, M. I. (1999). Cortical surface-based analysis. I. Segmentation and surface reconstruction. *NeuroImage*, *9*(2), 179–194.

Damasio, A. R. (1989). Time-locked multiregional retroactivation: a systems-level proposal for the neural substrates of recall and recognition. *Cognition*, *33*(1-2), 25–62.

Dumoulin, S. O., & Wandell, B. A. (2008). Population receptive field estimates in human visual cortex. *NeuroImage*, *39*(2), 647–660.

Esteban, O., Blair, R., Markiewicz, C. J., Berleant, S. L., Moodie, C., Ma, F., Isik, A. I., Erramuzpe, A., Kent, J. D., Goncalves, M., & Others. (2018). fMRIPrep. Software. *Zenodo*.

Esteban, O., Markiewicz, C. J., Blair, R. W., Moodie, C. A., Isik, A. I., Erramuzpe, A., Kent, J. D., Goncalves, M., DuPre, E., Snyder, M., Oya, H., Ghosh, S. S., Wright, J., Durnez, J., Poldrack, R. A., & Gorgolewski, K. J. (2019). fMRIPrep: a robust preprocessing pipeline for functional MRI. *Nature Methods*, *16*(1), 111–116.

Favila, S. E., & Aly, M. (2023). Hippocampal mechanisms resolve competition in memory and perception. *bioRxiv.org: The Preprint Server for Biology*. https://doi.org/10.1101/2023.10.09.561548

Favila, S. E., Kuhl, B. A., & Winawer, J. (2022). Perception and memory have distinct spatial tuning properties in human visual cortex. *Nature Communications*, *13*(1), 5864.

Favila, S. E., Samide, R., Sweigart, S. C., & Kuhl, B. A. (2018). Parietal representations of stimulus features are amplified during memory retrieval and flexibly aligned with top-down goals. *The Journal of Neuroscience: The Official Journal of the Society for Neuroscience*, *38*(36), 7809–7821.

Frankland, P. W., & Bontempi, B. (2005). The organization of recent and remote memories. *Nature Reviews. Neuroscience*, *6*(2), 119–130.

Gardner, J. L., Sun, P., Waggoner, R. A., Ueno, K., Tanaka, K., & Cheng, K. (2005). Contrast adaptation and representation in human early visual cortex. *Neuron*, *47*(4), 607–620.

Gilbert, C. D., & Sigman, M. (2007). Brain states: top-down influences in sensory processing. *Neuron*, *54*(5), 677–696.

Gordon, A. M., Rissman, J., Kiani, R., & Wagner, A. D. (2014). Cortical reinstatement mediates the relationship between content-specific encoding activity and subsequent recollection decisions. *Cerebral Cortex* , *24*(12), 3350–3364.

Gorgolewski, K., Burns, C. D., Madison, C., Clark, D., Halchenko, Y. O., Waskom, M. L., & Ghosh, S. S. (2011). Nipype: a flexible, lightweight and extensible neuroimaging data processing framework in python. *Frontiers in Neuroinformatics*, *5*, 13.

Gorgolewski, K. J., Auer, T., Calhoun, V. D., Craddock, R. C., Das, S., Duff, E. P., Flandin, G., Ghosh, S. S., Glatard, T., Halchenko, Y. O., Handwerker, D. A., Hanke, M., Keator, D., Li, X., Michael, Z., Maumet, C., Nichols, B. N., Nichols, T. E., Pellman, J., … Poldrack, R. A. (2016). The brain imaging data structure, a format for organizing and describing outputs of neuroimaging experiments. *Scientific Data*, *3*(1), 1–9.

Gorgolewski, K. J., Nichols, T., Kennedy, D. N., Poline, J.-B., & Poldrack, R. A. (2018). Making replication prestigious. *The Behavioral and Brain Sciences*, *41*, e131.

Greve, D. N., & Fischl, B. (2009). Accurate and robust brain image alignment using boundary-based registration. *NeuroImage*, *48*(1), 63–72.

Halchenko, Y. O. et al. (2018). Open Source Software: Heudiconv. *Zenodo*, https://doi.org/10.5281/zenodo.1306159.

Himmelberg, M. M., Kurzawski, J. W., Benson, N. C., Pelli, D. G., Carrasco, M., & Winawer, J. (2021). Cross-dataset reproducibility of human retinotopic maps. *NeuroImage*, *244*, 118609.

Hubel, D. H., & Wiesel, T. N. (1965). Receptive fields and functional architecture in two nonstriate visual areas (18 and 19) of the cat. *Journal of Neurophysiology*, *28*, 229–289.

Hunter J, (2007). Matplotlib: A 2D Graphics Environment. *Computing in Science & Engineering*, *9*(3), 90-95

Jehee, J. F. M., Ling, S., Swisher, J. D., van Bergen, R. S., & Tong, F. (2012). Perceptual learning selectively refines orientation representations in early visual cortex. *The Journal of Neuroscience: The Official Journal of the Society for Neuroscience*, *32*(47), 16747–16753a.

Jenkinson, M., Bannister, P., Brady, M., & Smith, S. (2002). Improved optimization for the robust and accurate linear registration and motion correction of brain images. *NeuroImage*, *17*(2), 825–841.

Johns, L. C., Cannon, M., Singleton, N., Murray, R. M., Farrell, M., Brugha, T., Bebbington, P., Jenkins, R., & Meltzer, H. (2004). Prevalence and correlates of self-reported psychotic symptoms in the British population. *The British Journal of Psychiatry: The Journal of Mental Science*, *185*(4), 298–305.

Kim, H. (2011). Neural activity that predicts subsequent memory and forgetting: a meta-analysis of 74 fMRI studies. *NeuroImage*, *54*(3), 2446–2461.

Klein, A. (2017). *Mindboggle-101 templates (unlabeled images from a population of brains). Harvard Dataverse*.

Knierim, J. J. (2015). The hippocampus. *Current Biology: CB*, *25*(23), R1116–R1121.

Kosslyn, S. M., Ganis, G., & Thompson, W. L. (2001). Neural foundations of imagery. *Nature Reviews. Neuroscience*, *2*(9), 635–642.

Kosslyn, S. M., & Thompson, W. L. (2003). When is early visual cortex activated during visual mental imagery? *Psychological Bulletin*, *129*(5), 723–746.

Kuhl, B. A., & Chun, M. M. (2014). Successful remembering elicits event-specific activity patterns in lateral parietal cortex. *The Journal of Neuroscience: The Official Journal of the Society for Neuroscience*, *34*(23), 8051–8060.

Kuhl, B. A., Johnson, M. K., & Chun, M. M. (2013). Dissociable neural mechanisms for goal-directed versus incidental memory reactivation. *The Journal of Neuroscience: The Official Journal of the Society for Neuroscience*, *33*(41), 16099–16109.

Kuhl, B. A., Rissman, J., Chun, M. M., & Wagner, A. D. (2011). Fidelity of neural reactivation reveals competition between memories. *Proceedings of the National Academy of Sciences of the United States of America*, *108*(14), 5903–5908.

Kwak, Y., & Curtis, C. E. (2022). Unveiling the abstract format of mnemonic representations. *Neuron*, *110*(11), 1822–1828.e5.

Lanczos, C. (1964). Evaluation of Noisy Data. *Journal of the Society for Industrial and Applied Mathematics Series B Numerical Analysis*, *1*(1), 76–85.

Lee, T. S., & Mumford, D. (2003). Hierarchical Bayesian inference in the visual cortex. *Journal of the Optical Society of America. A, Optics, Image Science, and Vision*, *20*(7), 1434–1448.

Lee, T. S., Mumford, D., Romero, R., & Lamme, V. A. (1998). The role of the primary visual cortex in higher level vision. *Vision Research*, *38*(15-16), 2429–2454.

Ling, S., Jehee, J. F. M., & Pestilli, F. (2015). A review of the mechanisms by which attentional feedback shapes visual selectivity. *Brain Structure & Function*, *220*(3), 1237–1250.

Linton, P., Heeger, D. J., Movshon, T., Muckli, L., Nienborg, H., Papale, P., Parker, A., Petro, L., Roelfsema, P., Talluri, B., Vetter, P., Xue, C., Zhaoping, L., & Kriegeskorte, N. (2024). *Is V1 a Cognitive Map?* https://doi.org/10.31219/osf.io/guf93

Markov, N. T., Vezoli, J., Chameau, P., Falchier, A., Quilodran, R., Huissoud, C., Lamy, C., Misery, P., Giroud, P., Ullman, S., Barone, P., Dehay, C., Knoblauch, K., & Kennedy, H. (2014). Anatomy of hierarchy: feedforward and feedback pathways in macaque visual cortex: Cortical counterstreams. *The Journal of Comparative Neurology*, *522*(1), 225–259.

Marr, D. (2010). *Vision: A computational investigation into the human representation and*

processing of visual information. MIT Press.

Maunsell, J. H. R., & Cook, E. P. (2002). The role of attention in visual processing. *Philosophical Transactions of the Royal Society of London. Series B, Biological Sciences*, *357*(1424), 1063–1072.

McClelland, J. L., McNaughton, B. L., & O'Reilly, R. C. (1995). Why there are complementary learning systems in the hippocampus and neocortex: insights from the successes and failures of connectionist models of learning and memory. *Psychological Review*, *102*(3), 419–457.

Mohsenzadeh, Y., Mullin, C., Oliva, A., & Pantazis, D. (2019). The perceptual neural trace of memorable unseen scenes. *Scientific Reports*, *9*(1), 6033.

Naselaris, T., Olman, C. A., Stansbury, D. E., Ugurbil, K., & Gallant, J. L. (2015). A voxel-wise encoding model for early visual areas decodes mental images of remembered scenes. *NeuroImage*, *105*, 215–228.

Pedregosa, F., Varoquaux, G., Gramfort, A., Michel, V., Thirion, B., Grisel, O., Blondel, M., Louppe, G., Prettenhofer, P., Weiss, R., Weiss, R. J., Vanderplas, J., Passos, A., Cournapeau, D., Brucher, M., Perrot, M., & Duchesnay, E. (2011). Scikit-learn: Machine Learning in Python. *Journal of Machine Learning Research: JMLR*, *abs/1201.0490*. https://doi.org/10.5555/1953048.2078195

Polyn, S. M., Natu, V. S., Cohen, J. D., & Norman, K. A. (2005). Category-specific cortical activity precedes retrieval during memory search. *Science (New York, N.Y.)*, *310*(5756), 1963–1966.

Prince, J. S., Charest, I., Kurzawski, J. W., Pyles, J. A., Tarr, M. J., & Kay, K. N. (2022). Improving the accuracy of single-trial fMRI response estimates using GLMsingle. *eLife*, *11*. https://doi.org/10.7554/eLife.77599

Reuter, M., Rosas, H. D., & Fischl, B. (2010). Highly accurate inverse consistent registration: a

robust approach. *NeuroImage*, *53*(4), 1181–1196.

Roediger, H. L., 3rd, & Butler, A. C. (2011). The critical role of retrieval practice in long-term retention. *Trends in Cognitive Sciences*, *15*(1), 20–27.

Rust, N. C., & Mehrpour, V. (2020). Understanding image memorability. *Trends in Cognitive Sciences*, *24*(7), 557–568.

Schacter, D. L. (1999). The seven sins of memory: Insights from psychology and cognitive neuroscience. *The American Psychologist*, *54*(3), 182–203.

Schacter, D. L., Norman, K. A., & Koutstaal, W. (1998). The cognitive neuroscience of constructive memory. *Annual Review of Psychology*, *49*, 289–318.

Teeuwen, R. R. M., Wacongne, C., Schnabel, U. H., Self, M. W., & Roelfsema, P. R. (2021). A neuronal basis of iconic memory in macaque primary visual cortex. *Current Biology: CB*, *31*(24), 5401–5414.e4.

Tootell, R. B., Hadjikhani, N., Hall, E. K., Marrett, S., Vanduffel, W., Vaughan, J. T., & Dale, A. M. (1998). The retinotopy of visual spatial attention. *Neuron*, *21*(6), 1409–1422.

Tünçok, E., Carrasco, M., & Winawer, J. (2024). Spatial attention alters visual cortical representation during target anticipation. In *bioRxiv*. https://doi.org/10.1101/2024.03.02.583127

Tustison, N. J., Avants, B. B., Cook, P. A., Zheng, Y., Egan, A., Yushkevich, P. A., & Gee, J. C. (2010). N4ITK: improved N3 bias correction. *IEEE Transactions on Medical Imaging*, *29*(6), 1310–1320.

The pandas development team. (2024). pandas-dev/pandas: Pandas (v2.2.1). Zenodo. https://doi.org/10.5281/zenodo.10697587

Uncapher, M. R., & Rugg, M. D. (2009). Selecting for memory? The influence of selective attention on the mnemonic binding of contextual information. *The Journal of Neuroscience: The Official Journal of the Society for Neuroscience*, *29*(25), 8270–8279.

Uncapher, M. R., & Wagner, A. D. (2009). Posterior parietal cortex and episodic encoding: insights from fMRI subsequent memory effects and dual-attention theory. *Neurobiology of Learning and Memory*, *91*(2), 139–154.

Virtanen, P., Gommers, R., Oliphant, T. E., Haberland, M., Reddy, T., Cournapeau, D., Burovski, E., Peterson, P., Weckesser, W., Bright, J., van der Walt, S. J., Brett, M., Wilson, J., Millman, K. J., Mayorov, N., Nelson, A. R. J., Jones, E., Kern, R., Larson, E., … van Mulbregt, P. (2020). SciPy 1.0: fundamental algorithms for scientific computing in Python. *Nature Methods*, *17*(3), 261–272.

Vo, V. A., Sutterer, D. W., Foster, J. J., Sprague, T. C., Awh, E., & Serences, J. T. (2022). Shared representational formats for information maintained in working memory and information retrieved from long-term memory. *Cerebral Cortex* , *32*(5), 1077–1092.

Wager, T. D., Jonides, J., & Reading, S. (2004). Neuroimaging studies of shifting attention: a meta-analysis. *NeuroImage*, *22*(4), 1679–1693.

Waskom, M. L., (2021). seaborn: statistical data visualization. Journal of Open Source Software, 6(60), 3021, https://doi.org/10.21105/joss.03021

Wheeler, M. E., Petersen, S. E., & Buckner, R. L. (2000). Memory's echo: vivid remembering reactivates sensory-specific cortex. *Proceedings of the National Academy of Sciences of the United States of America*, *97*(20), 11125–11129.

Williams, M. A., Baker, C. I., Op de Beeck, H. P., Shim, W. M., Dang, S., Triantafyllou, C., & Kanwisher, N. (2008). Feedback of visual object information to foveal retinotopic cortex. *Nature Neuroscience*, *11*(12), 1439–1445.

Woodry, R., Curtis, C. E., & Winawer, J. (2025). Feedback scales the spatial tuning of cortical responses during both visual working memory and long-term memory. *The Journal of Neuroscience: The Official Journal of the Society for Neuroscience*. https://doi.org/10.1523/JNEUROSCI.0681-24.2025

Yoshor, D., Ghose, G. M., Bosking, W. H., Sun, P., & Maunsell, J. H. R. (2007). Spatial attention does not strongly modulate neuronal responses in early human visual cortex. *The Journal of Neuroscience: The Official Journal of the Society for Neuroscience*, *27*(48), 13205–13209.

Young, D. R., & Bellezza, F. S. (1982). Encoding variability, memory organization, and the repetition effect. *Journal of Experimental Psychology. Learning, Memory, and Cognition*, *8*(6), 545–559.

Zhang, Y., Brady, J. M., & Smith, S. M. (2001). An hmrf-em algorithm for partial volume segmentation of brain mri fmrib technical report tr01yz1. *Brain: A Journal of Neurology*. https://www.fmrib.ox.ac.uk/datasets/techrep/tr01yz1/tr01yz1.pdf

Zokaei, N., Board, A. G., Manohar, S. G., & Nobre, A. C. (2019). Modulation of the pupillary response by the content of visual working memory. *Proceedings of the National Academy of Sciences of the United States of America*, *116*(45), 22802–22810.